METHODS OF CALCULATIONS

CoMFA Study

1. Biological data

1.1 Pyrimethamine

Twenty-three Pyr derivatives used for the CoMFA study were selected from Kamchonwongpaisan *et. al*. as shown in Table 1. There are three substitute positions, **X** (meta-position), **Y** (para-position) and **R** as shown in Figure 10. The eighteen compounds served as the training set. In addition, five compounds (compound number **2**, **5**, **9**, **10**, **23**) that were selected from the diversity and ranges of biological activities were kept to evaluate the predictive power of the models as the test set. For each set of biological data, the inhibition constant, K_i (*n*M) for inhibiting quadruple mutant (Asn51Ile, Cys59Arg, Ser108Asn, Ile164Leu) *Pf*DHFR, was measured *in vitro* under the same experimental conditions. Consequently, *in vitro* antimalarial activities were converted into the corresponding pK_i (-logK_i) values. These values were used as dependent variables in the CoMFA study.

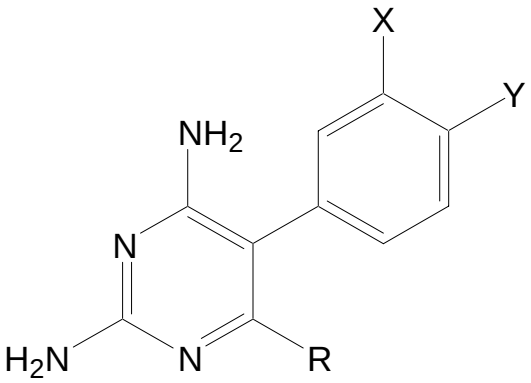

Figure 10 Template structure of 5-phenyl-2,4-diaminoPyrimidine derivatives

Table 1 Data set used for CoMFA analysis with K_i (*n*M) and pK_i values in the quadruple mutant (Asn51Ile, Cys59Arg, Ser108Asn, Ile164Leu) of *Pf*DHFR.

Comp	**X**	**Y**	**R**	K_i **(*n*M)**	pK_i
1 (P1)	H	Cl	Et	385	6.41
2 (P15)[a]	-OCH_2O-		Et	269	6.57
3 (P17)	H	Me	Et	284	6.55
4 (P13)	Cl	Cl	Et	53	7.27
5 (P20)[a]	H	H	Et	32	7.49
6 (P30)	Cl	H	Et	3.3	8.48
7 (P16)	H	Cl	$(CH_2)_3COOMe$	360	6.44
8 (P26)	H	H	$(CH_2)_3COOMe$	24	7.62
9 (P29)[a]	Cl	H	$(CH_2)_3COOMe$	2.7	8.57
10 (P12)[a]	H	Cl	$(CH_2)_3Ph$	170	6.77
11 (P33)	H	H	$(CH_2)_3Ph$	4.7	8.33
12 (P31)	Cl	H	$(CH_2)_3Ph$	2	8.70
13 (P45)	H	H	$(CH_2)_3OH$	549	6.26
14 (P41)	Cl	H	$(CH_2)_3OH$	57	7.24
15 (P46)	H	H	$(CH_2)_3OCOCH_3$	237	6.62
16 (P42)	Cl	H	$(CH_2)_3OCOCH_3$	31.4	7.50
17 (P47)	H	H	$(CH_2)_3OCOC_6H_5$	14	7.85
18 (P43)	Cl	H	$(CH_2)_3OCOC_6H_5$	3.6	8.44
19 (P39)	H	H	nC_6H_{13}	1.4	8.85
20 (P44)	Cl	H	$(CH_2)_3OCOOCH_2C_6H_5$	3.6	8.44
21 (P38)	Cl	H	Me	14	7.85
22 (P32)	Cl	H	$(CH_2)_3C_6H_4$-(*p*-OMe)	2	8.70
23 (P40)[a]	Cl	H	$(CH_2)_2O(CH_2)_3OPh$	1.7	8.77

[a]Test set compounds

1.2 Cyclogunail

A set of Twenty-five Cyc derivatives consisting four structural modifications (see in Figure 11) with inhibition constants (K_i) for binding with wild type and the quadruple mutant type (Asn51Ile, Cys59Arg, Ser108Asn, Ile164Leu) *Pf*DHFRs (Kamchonwongpaisan, *et al*., 2004) was selected for CoMFA study as listed in Table 2. A training set of 20 compounds was used and five antimalarials, selected from various ranges of biological activity, were kept as a test set for evaluating the model. A dependent variable in CoMFA was defined as pK_i (-logK_i), where K_i values were measured *in vitro* under the same experimental conditions.

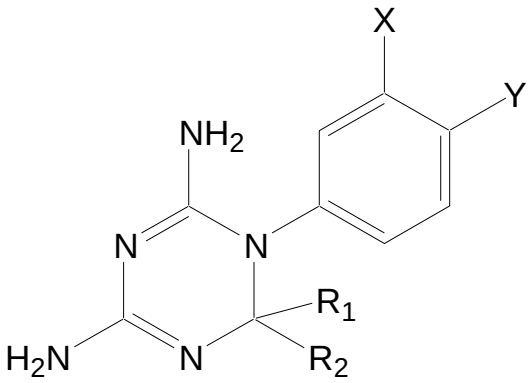

Figure 11 Template structure of 1,3,5 dihydrotriazine derivatives

Table 2 Data set used for CoMFA analysis with their K_i (nM) and pK_i (M) values in the wild type (wt) and quadruple mutant (mut) *Pf*DHFR models.

Comp	**X**	**Y**	**R_1**	**R_2**	***K_i*(wt) (*n*M)**	**p*K_i*(wt)**	***K_i*(mut)[a] (*n*M)**	**p*K_i*(mut)**
1 (C21)	H	Cl	Me	Me	1.5	8.82	420	6.37
2 (C97)	Cl	H	Me	Me	3.0	8.52	25	7.60
3 (C66)[b,c]	H	Cl	Me	*n*Pr	3.5	8.45	4432	5.35
4 (C433)	Cl	H	Me	*i*Pr	25.5	7.59	472	6.32

Table 2 (Continued)

Cpd	X	Y	R_1	R_2	K_i(wt) (*n*M)	pK_i(wt)	K_i(mut)[a] (*n*M)	pK_i(mut)
5 (C22)	H	Cl	Me	*i*Pr	36.5	7.44	> 10000	5.00
6 (C434)	Cl	H	Me	*n*Pr	4.6	8.34	39.4	7.40
7 (C71)	H	Cl	Me	*n*Hex	0.6	9.22	69.2	7.16
8 (C435)[c]	Cl	H	Me	*n*Hex	2.4	8.62	15.9	7.79
9 (C17)	H	Cl	H	Me	4.1	8.38	2427	5.61
10 (C248)[b]	Cl	H	H	Me	10.2	7.99	14.3	7.84
11 (C53)	H	Cl	H	C_6H_5	4.5	8.34	2436	5.61
12 (C96)	Cl	H	H	C_6H_5	11.7	7.93	984	6.01
13 (C121)	H	Cl	H	4-$C_6H_5OC_6H_4$	0.4	9.39	222	6.65
14 (C138)	Cl	H	H	4-$C_6H_5OC_6H_4$	0.7	9.15	1.3	8.88
15 (C133)[b,c]	H	Cl	H	3-$C_6H_5OC_6H_4$	0.5	9.30	239	6.62
16 (C110)	Cl	H	H	3-$C_6H_5OC_6H_4$	1.1	8.96	5.8	8.23
17 (C111)	H	Cl	H	3-C6H5$CH_2OC_6H_4$	0.7	9.15	638	6.19
18 (C185)[c]	Cl	H	H	3-C6H5$CH_2OC_6H_4$	2.3	8.64	7.7	8.11
19 (C188)[b]	H	Cl	H	3-(4-ClC_6H_4O)C_6H_4	1.4	8.85	121	6.92
20 (C143)	Cl	H	H	3-(4-ClC_6H_4O)C_6H_4	1.3	8.88	8.0	8.09
21 (C372)	Cl	H	H	*n*C_7H_{15}	2.7	8.56	0.8	9.09
22 (C229)[b]	Cl	H	H	4-$PrOC_6H_4$	3.3	8.48	2.7	8.57
23 (C186)[c]	Cl	H	H	3-(3,5-$Cl_2C_6H_3O$)C_6H_4	1.8	8.74	2.7	8.57
24 (C313)	Cl	H	H	3-[2,4,5-$Cl_3C_6H_2O(CH_2)_3O$]C_6H_4	4.0	8.40	4.5	8.34
25 (C299)	Cl	H	H	3-(3-$CF_3C_6H_4O$)C_6H_4	2.7	8.57	4.8	8.32

[a] quadruple mutation (N51I + C59R + S108N + I164L) of *Pf*DHFR

[b] test set compounds for wild type *Pf*DHFR CoMFA model

c test set compounds for quadruple mutant type *Pf*DHFR CoMFA model

2. Structural Construction

Three-dimensional structure building was constructed using the Sybyl 7.0 program package on a Silicon Graphics Octane2 workstation at the National Electronics and Computer Technology Center of Thailand (NECTEC). The structures of Pyr derivatives were built using the SKETCH module in Sybyl. The skeleton and conformation of Pyr (compound **1**) was extracted from the crystal structure of a Pyr complex with double mutant *Pf*DHFR with PDB code 1J3J (Yuvaniyama, *et al*., 2003). The other molecules were built taking compound **1** as a template and changing their substituents. The basic scaffold of examined compounds exhibits a fair degree of symmetry, which could lead to different compounds being positioned in different ways in the binding site, or even having multiple modes of binding contributing to the interaction with the binding site. There are two possible modes of binding of X substitutions of Pyr derivatives. However, when considering the space available as shown in Figure 12, there is limited space caused by NAD cofactor. Therefore, in this present work, the X substituent at position 3 was selected to construct CoMFA model for the Pyr derivatives.

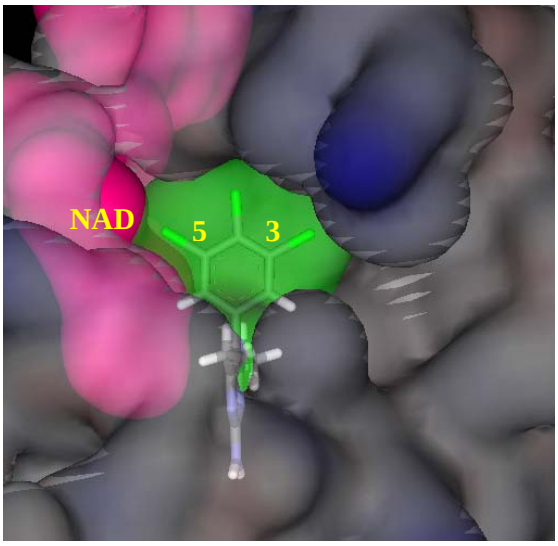

Figure 12 Example of graphic representation of the binding site with Pyrimethamine (compound 4), the cofactor NAD was presented and caused space limitation for position 5 substitution.

All Cyc derivatives were also built in the SKETCH module of Sybyl program using the same template as used for Pyr derivatives. The structural of Cyc derivatives were constructed based on the same Pyr basic scaffold of multiple modes of binding contributing to the interaction with the binding site. However, the conformation of Cyc derivatives was investigation before 3D-structural constructions. Based on the pocket limitations, then the R-conformation form was selected to bulid Cyc chiral derivatives. Consequently, a geometry optimization was carried out using a Tripos force field, and then, a Gasteiger-Hückle charge was also employed in Sybyl7.0 program.

3. CoMFA Alignments

An atom-base superimposition alignment was applied to Pyr and Cyc compounds using their common templates as see with the asterisks in Figure 13 and 14, respectively.

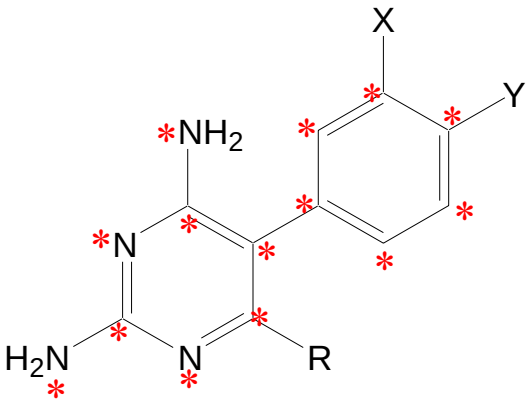

Figure 13 Template alignment of Pyr derivatives shown with the asterisks

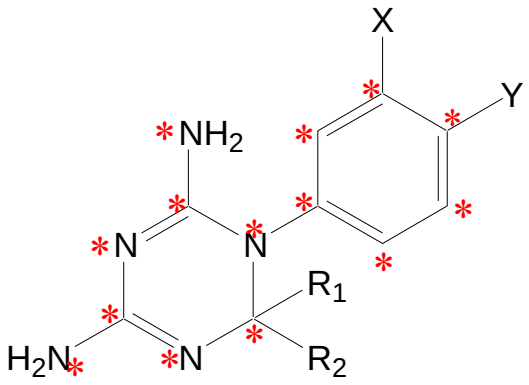

Figure 14 Template alignment of Cyc derivatives displayed with the asterisks

The 3D cubic lattices, with 2 Å grid spacing, were generated around the aligned compounds based on the molecular volume of the structure. The lattices were defined automatically, and were extended by 4.0 Å in all directions. Three types of probe atoms were placed at each lattice point, namely sp^3 carbon atom with +1 charge, sp^3 oxygen atom with –1 charge and H atom with +1 charge. The interactions of the steric and electrostatic fields with each atom in the molecule were calculated using CoMFA standard scaling. The default value of 30 kcal/mol was used as the maximum electrostatic and steric energy cutoff. The CoMFA fields were scaled by CoMFA-STD method in Sybyl. Then a partial least squares technique (PLS) was employed to derive a CoMFA model expressing the correlation between the steric and electrostatic properties and the biological activities. The orthogonal latent variables were extracted by the NIPALS algorithm and subjected to full cross-validation with the leave-one-out method (LOO). In order to speed up the analysis and reduce the amount of noise, the minimum sigma value was set to 2.0 kcal/mol as a default. The analyses were carried out with a maximum of six components, then using the number of component (noc) at which the difference in the r^2_{cv} value compared to the next one was less than 0.05.

4. CoMFA Predictive Ability

The predictive ability of the model that was derived from the training set is expressed by the cross-validation predictive (r^2_{cv}) value. The r^2_{cv} value is defined as

$$r_{cv}^2 = 1.0 - \frac{PRESS}{SSY} \quad (1)$$

where, SSY is the variance of the biological activities around the mean value, and PRESS is the prediction error sum of squares derived from the LOO.

$$PRESS = \sum_y (y_{pred} - y_{actual})^2 \quad (2)$$

$$SSY = \sum_y (y_{actual} - y_{mean})^2 \quad (3)$$

The uncertainty of the prediction is defined as

$$S_{PRESS} = \sqrt{\frac{PRESS}{n-k-1}} \quad (4)$$

where *k* is the number of variables in the model and n is the number of compounds used in the study (Golbraikh, *et al*., 2002, Nilsson, *et al*., 1997, Hannongbua, *et al*., 2001).

Quantum Chemical Calculations Study

1. Model Set-up

1.1 Pyrimethamine

In order to investigate specific interaction of different potency of Pyr derivatives in quadruple mutant DHFR, particular interaction was determined by quantum chemical calculations. According to comparison between double mutant complex with Pyr (1J3J) and quadruple mutant complex with WR99210 (1J3K) structures (Yuvaniyama, *et al*., 2003) superimposition, it was found that the binding sites are quite similar with RMS = 0.435 Å as shown in Figure 15.

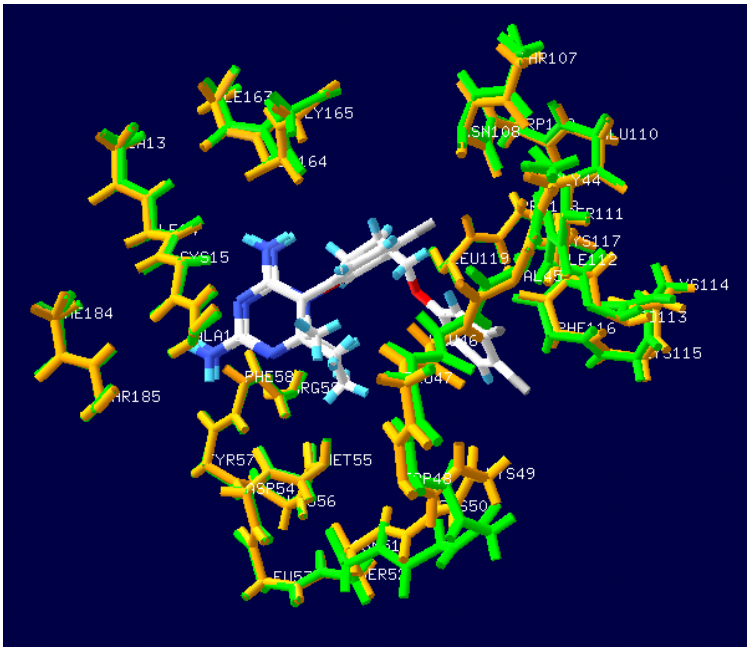

Figure 15 The backbone superimposition between the X-ray *Pf*DHFR/WR99210 complex structures of quadruple mutant (PDB entry 1J3K shown in green color) and *Pf*DHFR/Pyr double mutant (PDB entry 1J3J shown in orange color), indicating the similarity binding position of both two inhibitors.

Due to there being no Pyr/quadruple mutant DHFR available, therefore, in this study, we proposed Pyr and quadruple mutant complex, based on atom superposition. Considering the graphical backbone superimpostion, it can be implied that WR99210 and Pyr oriented in the same binding position, therefore, Pyr can be adapted into the quadruple mutant type *Pf*DHFR to find the estimated particular interaction energy. Based on inhibitor comparison, the selected inhibitors were compounds **1** (Pyr drug) and **6** according to their similar structures, but different K_i values (see in Table 1). Compound **1** represented a resistance to quadruple mutant *Pf*DHFR while compound **6**, Cl substituent at **X**, gave a good K_i for this enzyme. The model systems contained compounds **1** or **6** and surrounding residues in the binding pocket with at least one atom interacting with any atoms of inhibitor within the interatomic distance approximately 4 Å that covered van der Waal interactions. The 23 selected residues were Ile14, Cys15, Ala16, Val45, Leu46, Trp48, Cys50, Ile51, Asp54, Met55, Tyr57, Phe58, Arg59, Met 104, Asn108, Ser111, Ile112, Pro113, Phe116, Leu119, Leu164, Gly165 and Thr185. The four mutations, Asn51Ile, Cys59Arg, Ser108Asn and Ile164Leu, were also included in the system setup. The 2D scheme of the adopted model system of the inhibitor bound to the mutant *Pf*DHFR binding site is shown in Figure 16. In addition, the backbone of eleven inserted residues, 47, 49, 52, 53, 56, 109, 110, 114, 115, 117 and 118, were added into the system to complete the connection between the amino acids in the cutting chains. The N- and C-terminals were capped with a methyl amino group (-$NHCH_3$) and an acetyl group (CH_3CO-), respectively, which were retained from the backbone geometries of the nearby residues. Thus, the hydrogen atoms were added to the starting system using Sybyl7.0. Partial optimizations were performed by using the semiempirical PM3 method, implemented in the Gaussian 03 program (Frisch, *et al.*, 2003) based on the 'heavy atoms fixing' approximation. Therefore, only H atoms of amino acids and all atoms of the inhibitor were optimized.

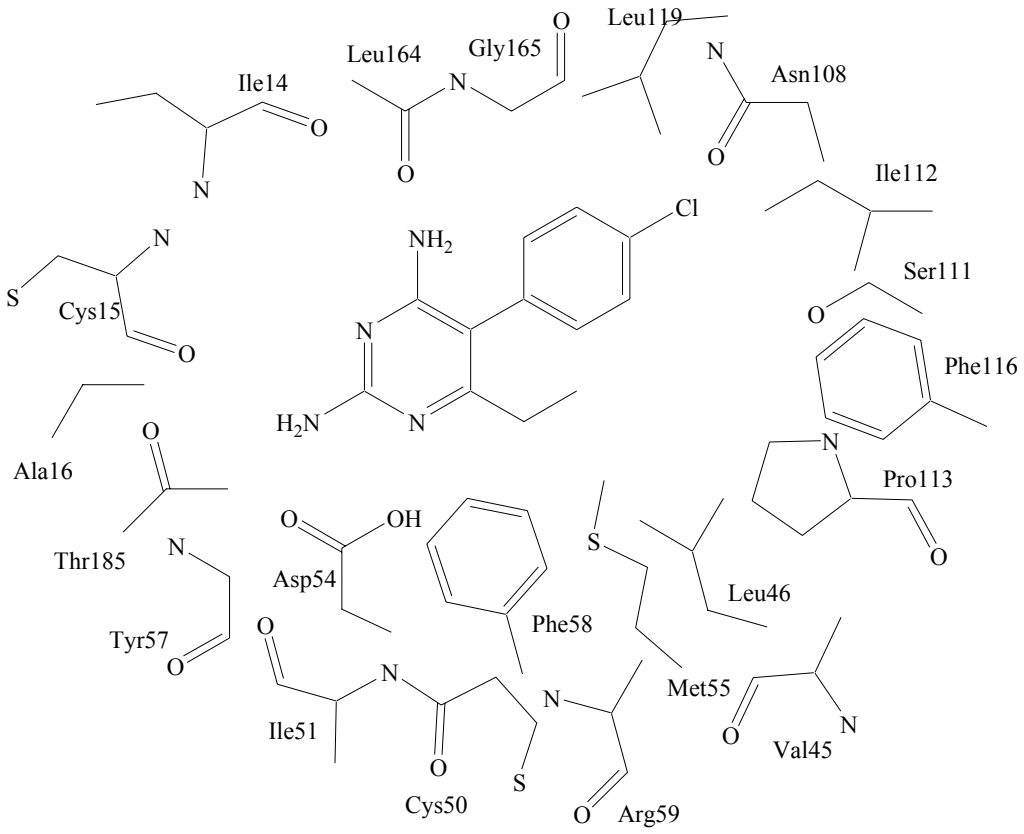

Figure 16 The 2D scheme of the adopted model system of Pyr inhibitor bound to the quadruple mutant type (Asn51Ile, Cys59Arg, Ser108Asn, and Ile164Leu) of *Pf*DHFR binding site.

1.2 Cycloguanil

Based on our objectives, a comparison of the role of the amino acids surrounding the binding pocket of Cyc in the wild type and the quadruple mutant type *Pf*DHFRs was investigated using AMBER molecular mechanic minimizations and quantum chemical calculations. So, the wild type and the quadruple mutant type *Pf*DHFRs with the Cyc inhibitor were constructed from the WR99210/wild type *Pf*DHFR and the WR99210/quadruple mutant type *Pf*DHFR x-ray complex structures with PDB code 1J3I and 1J3K, respectively (Yuvaniyama, *et al*., 2003). The proteins were added to the missing residues using Swiss-Pdb Viewer 3.7 program. The Cyc structure was fully optimized at the B3LYP/6-31G(*) level of calculations, and then

the RESP electrostatic charges (Cornell, *et al*., 1993) of all atoms in the Cyc inhibitor were also calculated using the Gaussian 03 package. The resultant structural and electrostatic charges were used to prepare the molecular mechanical Amber force field parameters using the Antech Amber module. For NADPH cofactor AMBER parameters (Cummins, *et al*., 1991) were taken from AMBER Parameter Database (http://www.pharmacy. manchester.ac.uk/bryce/amber/). The TIP3PBOX water molecules were used to solvate both complexes. Four chloride ions were added to neutralize the system. The minimization process of the complex structures was performed to eradicate bad contacts and to relax the complexed models. A cutoff distance of 12 Å was set for the non-bonded pair interactions. All molecular mechanical minimizations were carried out using the AMBER 9.0 simulation package (Case, *et al*., 2006).

The obtained molecular mechanical structures of the wild type and the quadruple mutant type *Pf*DHFRs complexed with the Cyc ligand were used as the starting geometry of the particular interaction energy calculations at the molecular level for the Cyc inhibitor with respect to both target enzymes. All residues located with at least one atom interacting with any atoms of the inhibitor within the interatomic distance of 4 Å were selected to calculate the interaction energy with the inhibitor based on quantum chemical calculations. The twenty selected residues were Ile14, Cys15, Ala16, Val45, Leu46, Trp48, Cys50, Asn51Ile, Asp54, Met55, Tyr57, Phe58, Met104, Ser108Asn, Ser111, Ile112, Leu119, Ile164Leu, Gly165 and Thr185. The Cys59Arg, Pro113 and Phe116 were also included into the systems for comparing their particular interaction enrgies contributed to Cyc and WR99210. The 2D scheme of twenty-three residues was shown in Figure 17. In addition, the backbond amino acids of fourteen inserted residues, Pro47, Lys49, Ser52, Leu53, Lys56, Gly105, Arg106, Thr107, Trp109, Glu110, Lys114, Lys115, Lys117 and Pro118, were added into the system to complete the connection between the amino acids in the cutting chains.The N- and C-terminals were capped with a methyl amino group (-$NHCH_3$) and an acetyl group (CH_3CO-), respectively, which were retained from the backbone geometries of the nearby residues. Geometry optimization of the hydrogen atoms was carried out based on the HF/6-31G(d,p) semiempirical level of

calculations, implemented in the Gaussian 03 program (Frisch, *et al*., 2003) running on a linux super cluster (4 CPU 3.2 GHz RAM 3.0 GB).

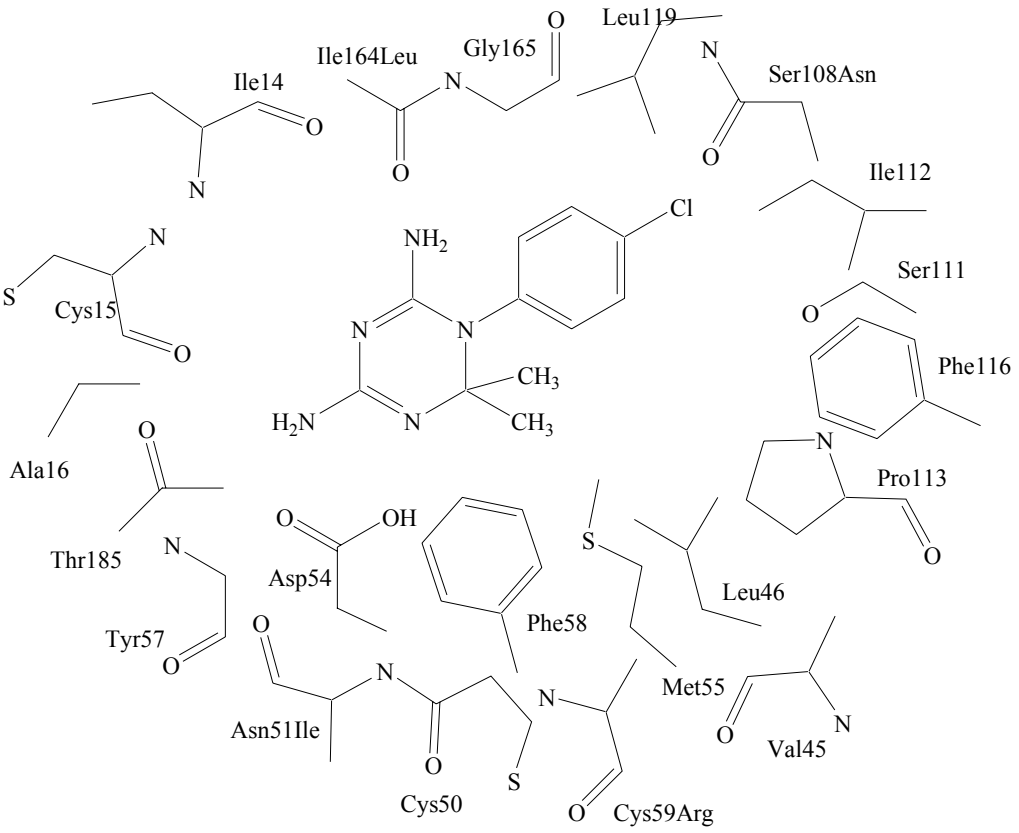

Figure 17 The 2D scheme of the adopted model system of Cyc bound to the wild type and quadruple mutant type *Pf*DHFR binding sites.

1.3 WR99210

The wild type and the quadruple mutant type *Pf*DHFR with the RW99210 inhibitor were constructed from the WR99210/wild type *Pf*DHFR and the WR99210/quadruple mutant type *Pf*DHFR x-ray complex structures with PDB code 1J3I and 1J3K, respectively (Yuvaniyama, *et al*., 2003). We also focused on WR99210 inhibitor and the residues in the binding pocket with at least one atom interacting with any atoms of inhibitor within the interatomic distance of 4 Å. There were twenty-three selected residues, Ile14, Cys15, Ala16, Val45, Leu46, Trp48,

Cys50, Asn51Ile, Asp54, Met55, Tyr57, Phe58, Cys59Arg, Met104, Ser108Asn, Ser111, Ile112, Pro113, Phe116, Leu119, Ile164Leu, Gly165 and Thr185 as shown 2D scheme in Figure 18.

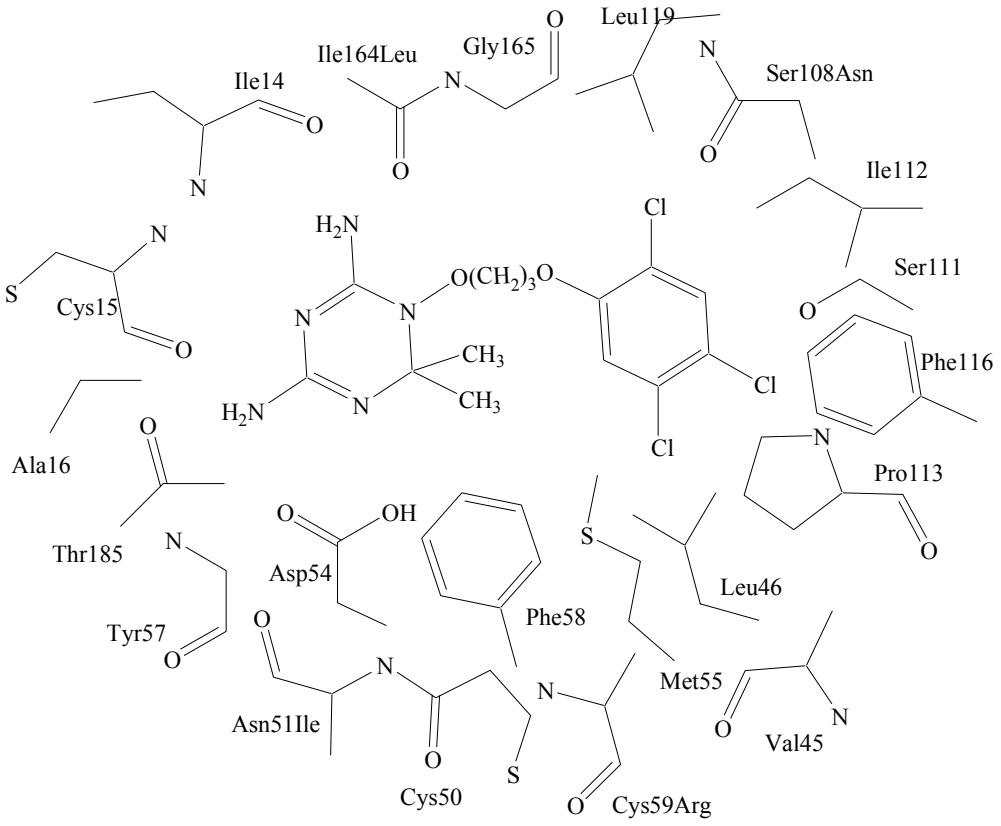

Figure 18 The 2D scheme of the adopted model system of flexible potent Cyc derivative, WR99210, bound to the *Pf*DHFR binding site.

Then, the N- and C-terminals were capped with a methyl amino group (-$NHCH_3$) and an acetyl group (CH_3CO-), respectively, which were retained from the backbone geometries of the nearby residues. Geometry optimization of the hydrogen atoms was carried out based on the HF/6-31G(d,p) semiempirical level of calculations which following the same steps of Pyr and Cyc system set-up.

2. Interaction Energy Calculations

The antifolate resulting geometries were used to provide different model systems of the antifolate inhibitor and the residues for high level of ab-initio MP2/6-31G(d,p) calculations, which then provided informations on the particular interaction energy between the inhibitor and each residue surrounding the binding site as shown in the interaction energy formula:

$$E^{INT}_{(\text{ligand}-\text{aminoacid})} = E^{AB}_{(\text{ligand}-\text{aminoacid})} - E^{A}_{(\text{ligand})} - E^{B}_{(\text{aminoacid})} \quad (5)$$

where A and B are the number of basis sets of ligands and amino acids, respectively, $E^{AB}_{(\text{ligand}-\text{aminoacid})}$ is the energy of the ligand-amino acid complex with the basis set of A plus B. $E^{A}_{(\text{ligand})}$ and $E^{B}_{(\text{aminoacid})}$ are the energies of the ligand and the amino acid with its number of basis sets.

Furthermore, the basis set superposition error based on the counterpoise scheme (BSSE-CP) of Boys-Bernardi (Boys, *et al.*, 1970) was also computed to define the interaction energy with BSSE as shown in equation 6:

$$E^{INT}_{(\text{ligand}-\text{aminoacid})} = E^{AB}_{(\text{ligand}-\text{aminoacid})} - E^{AB}_{(\text{ligand})} - E^{AB}_{(\text{aminoacid})} \quad (6)$$

where $E^{AB}_{(ligand)}$ and $E^{AB}_{(\text{aminoacid})}$ are the energies of the ligand and the amino acid, respectively, with the number of basis sets of A plus B (Saen-oon, *et al.*, 2005, Kuno, *et al.*, 2003 and 2006).

ONIOM3 Binding Energy Extrapolations

1. ONIOM model set-up

An ONIOM method, developed by Morokuma (Dapprich, *et al*., 1999, Morokuma, 2002; Morokuma, *et al*., 2006) has been applied to *Pf*DHFR/inhibitor. Simply put the concept of the ONIOM approach is to partition the large molecular system into onion-skin-like layers, using different combinations of the quantum chemical methods and molecular mechanics methods for different layers of the system partitioning

There were three systems which consisted of the three antifolates (Pyr, Cyc and WR99210) complexed with the same quadruple mutant *Pf*DHFR. The mutant *Pf*DHFR with Cyc and Pyr inhibitors were constructed from WR99210/quadruple mutant type *Pf*DHFR X-ray complex structures with PDB code 1J3K (Yuvaniyama, *et al*., 2003). The proteins were added the missing residues from 85 to 96 using Swiss-Pdb Viewer 3.7 program. All structural antifolate inhibitors were fully optimized at the B3LYP/6-31G(*) level of calculations, and then, calculated the RESP electrostatic charges (Cornell, *et al*., 1993) using the Gaussian 03 program package (Frisch, *et al*., 2003). The obtained structures and electrostatic charges were used for molecular mechanics calculations using Antech Amber module. Parameters of cofactor NADPH were taken from AMBER Parameter Database (Cummins, *et al*., 1991). The TIP3PBOX water molecules were used to solvate the complexes. Four chloride ions were added to neutralize the system. The minimization process of complex structures was performed to eradicate bad contacts and to relax the models. A cutoff distance of 12 Å was set for non-bonded pair interactions. The Particle Mesh Ewald (PME) method (Darden, *et al*., 1993) was employed to correct for electrostatic interactions. All bonds to hydrogen atoms were constrained by using the SHAKE algorithm. The simulation time step was set at 2 fs. The temperature of the model was gradually raised to 298 K for the first 100 ps, then, kept constant until 500 ps. The coordinates were saved every 1 ps, and the trajectories of 500 ps were analyzed with the Moil-

view program. All molecular dynamics simulations were carried out using the AMBER 9.0 simulation package (Case, *et al*., 2006), running on Linux PC 3.4 GHz.

The quadruple mutant *Pf*DHFR enzyme complexed with three types of antifolates systems were focused in this study. Due to the effect of mutated residues to binding affinity of antifolate inhibitors, we already performed quantum chemical calculations on the model systems which contained inhibitor and four mutated residues, Ile51, Arg59, Asn108 and Leu164, to find the interaction energy of each mutated residue contributed to the inhibitor.

The resultants of specific interaction energies of four mutated residues contributing to three antifolates were listed in Table 3. Considering the two mutated residues, Ile51 and Arg59 show slightly repulsive interactions with all inhibitors. Leu164 showed strong attractive energy values bacause its back bone amino acid produced H-bonded interaction with the amino group of inhibitor. The changing from Ser to Asn at the 108 position in quadruple mutant type enzyme showed the largest repulsive interaction energy with the rigid inhibitors, Pyr and Cyc, by approximately 4 kcal/mol. On the other hand, the potent WR99210 inhibitor exhibits attractive interaction. Asp54, the strongest interactions, was selected in the high level for keeping the electrostatic interaction with protonated antifolate inhibitors. Then Leu164 and Asn108 were included to add into the high level of calculations.

For intermediate layer, the residues located with at least one atom interacting with any atoms of the inhibitor within the interatomic distance of 4 Å were selected to set-up in the intermediate model of calculations. The outer layer of whole *Pf*DHFR enzyme was served as the real system as shown the ONIOM3 systems set-up and details of ONIOM3 calculations in Table 4.

Table 3 Interaction energies (kcal/mol) between three antifolate and four mutated residues of *Pf*DHFR using MP2/6-31G(d,p) level of calculations

Mutated residues	Interaction energy (kcal/mol)		
	Pyr	**Cyc**	**WR99210**
Ile51	0.044	0.127	0.149
Arg59	1.475	1.299	1.074
Asn108	3.921	4.329	-1.850
Leu164	-3.327	-3.457	-4.436
Asp54	-37.139	-39.770	-40.218

Table 4 Details of ONIOM3 layer partitions and level of calculations

Layer	**Detail of layer**	**Method of calculations**
Small	(**A**) inhibitor[a] + Asp54 + Asn108 + Leu164	*High*: B3LYP/6-31G(d,p)
Intermediate	(**AB**) A + 20 amino acids; Ile14, Cys15, Ala16, Val45, Leu46, Trp48, Cys50, Ile51, Met55, Tyr57, Phe58, Arg59, Met104, Ser111, Ile112, Pro113, Phe116, Leu119, Gly165 and Thr185	*Medium*: PM3 semiempirical
Real	(**ABC**) whole quadruple mutant *Pf*DHFR enzyme	*Low*: UFF molecular mechanics

[a] three type of antifolates, Pyr, Cyc and WR99210

The antifolate/quadruple mutant *Pf*HDFR complexes were divided into three parts as shown in Figure 19. The small layer, with ball and stick model, represents the binding of antifolate to effective mutated amino acids (Leu164 and Asn108) and strongest attractive amino acid (Asp54). These were treated at the high level of quantum chemical (HQ) calculations using density functional theory (B3LYP/6-31G(d,p)). The intermediate layer covers all amino acids of both chains of the antifolate lying within 4 Å from any atom of antifolate.

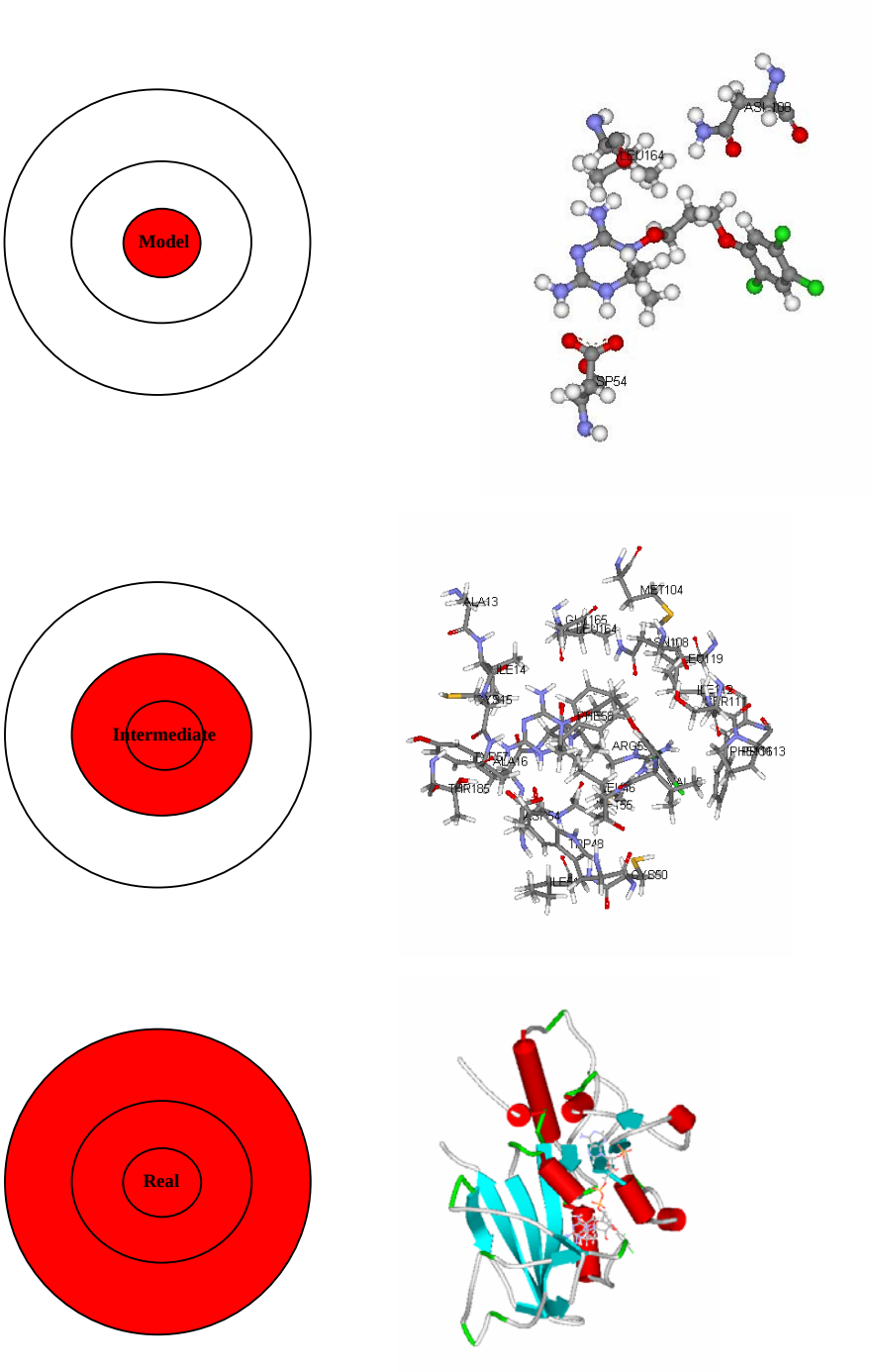

Figure 19 Schematic representation of the three-layer ONIOM; region of high level represented by ball and stick, medium level represented by pink stick and whole enzyme using low level of calculations

This layer was treated with the lower level of quantum chemical (LQ) calculations, a PM3 semiempirical method. The real layer takes into account the entire enzyme system. It was carried out by the molecular mechanics (MM) method using a universal force field or UFF.

2. ONIOM Energy Calculations

Figure 20 illustrates the basic concept of the three-layer ONIOM using in this study. The three-layer ONIOM(HQ:LQ:MM) energy is an approximation to the energy at the high level for the whole ligand/enzyme complex system.

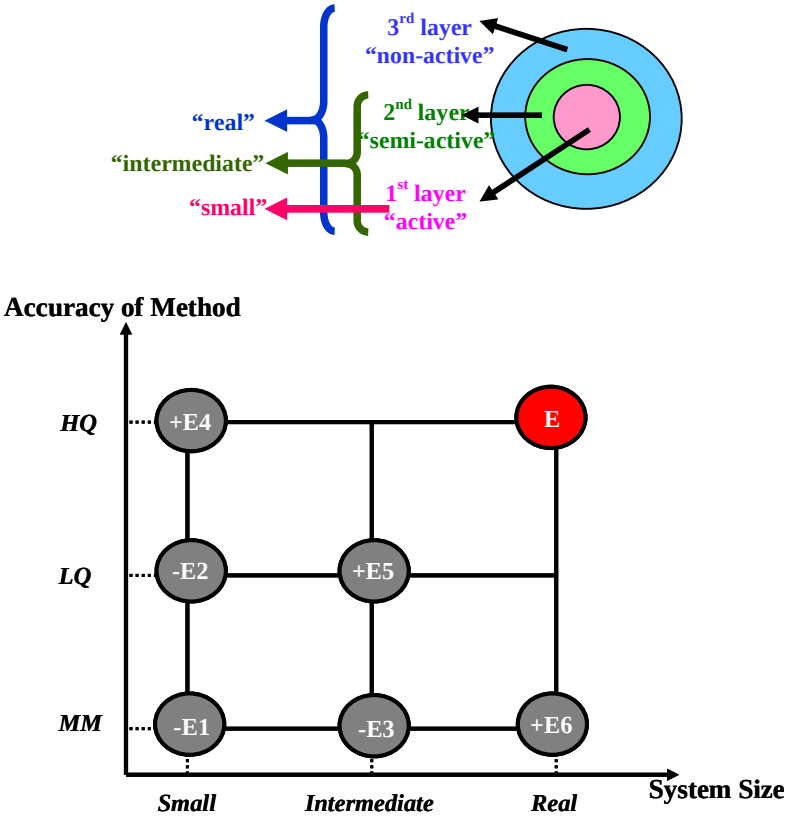

Figure 20 Extrapolation schematic representation of the three-layer ONIOM partitions and energy calculations.

Therefore, the extrapolated energy of real system at the high level of caluclations is given by

$$E^{HQ}_{real} = E^{MM}_{real} + E^{LQ}_{intermediate} + E^{HQ}_{small} - E^{MM}_{int\,ermediate} - E^{LQ}_{small} \quad \text{or} \qquad (7)$$

$$= E6 + E5 + E4 - E3 - E2 \qquad (8)$$

where E^{MM}_{real} denotes the *real* entire system, which is treated by UFF molecular mechanic calculations, while $E^{LQ}_{int\,ermediate}$ and $E^{MM}_{int\,ermediate}$ denote the part of the system partitioned to be the *intermediate* layers for which the energy are calculated at both PM3 and MM calculations. Here, E^{HQ}_{small} and E^{LQ}_{small} denote the *small* layer of the system partitioning, whose energy are calculated by B3LYP/6-31G(d,p) PM3 method, respectively.

In this study, the binding energy of three antifolates bound into the quaruple mutant type *Pf*DHFR was investigated using ONIOM extrapolations. Therefore, the binding energy ($\Delta E^{ONIOM}_{binding\ energy}$) between antifolate inhibitor and the quadruple mutant *Pf*DHFR enzyme was defined as following

$$\Delta E^{ONIOM}_{binding\ energy} = E^{ONIOM}_{complex} - E^{ONIOM}_{PfDHFR\text{-}enzyme} - E^{HQ}_{antifolate\text{-}inhibitor} \qquad (9)$$

where $E_{complex}$, $E_{PfDHFR\text{-}enzyme}$ and $E_{antifolate\text{-}inhibitor}$ represent the total energies of the antifolate/*Pf*DHFR complex, *Pf*DHFR enzyme and antifolate inhibitor, respectively. All configurations taken from the averaged molecular dynamics structures of the antifolate/*Pf*DHFR complex were used. The ONIOM calculations were carried out using the Gaussian 03 program package (Frisch, *et al*., 2003).